Original Paper

Optical spectroscopy of rare earth ions in glasses[1)]

Heike Ebendorff-Heidepriem and Doris Ehrt

Otto-Schott-Institut für Glaschemie, Friedrich-Schiller-Universität, Jena (Germany)

The relationships between host glass composition and optical properties of rare earth ions were studied by means of absorption and emission spectroscopy. Eu^{3+} and Tb^{3+} were found to be appropriate indicator ions for determining the properties of the local environment around rare earth ions. Er^{3+} and Nd^{3+} ions are widely used in lasers and amplifiers. The knowledge of the compositional influence on the spectroscopic parameters of rare earth ions enabled the modeling of the emission properties of important Er^{3+} and Nd^{3+} transitions in order to figure out the optimum host glasses. Fluoride phosphate and phosphate glasses are attractive candidates for lasers and amplifiers. In these glasses, the degree of covalency between the rare earth ions and surrounding ligands mainly affects the spectroscopic parameters of rare earth ions such as Judd-Ofelt parameters and electron-phonon coupling strength. The increase of the electron-phonon coupling strength with the phosphate content is responsible for the decrease of the Er^{3+} emission intensity at 540 nm. Otherwise, it increases the Er^{3+} emission intensity at 1.5 µm in the fluoride phosphate glasses. The lower microparameters of Nd^{3+} cross relaxation in phosphate glasses cause the higher lifetimes of the Nd^{3+} $^4F_{3/2}$ laser state at higher Nd^{3+} concentrations with respect to fluoride phosphate glasses. The energy transfer to OH groups in phosphate glasses decreases the lifetime and emission intensity of the laser state of both Er^{3+} and Nd^{3+} ions.

Optische Spektroskopie von Seltenerdionen in Gläsern

Die Beziehungen zwischen Wirtsglaszusammensetzung und optischen Eigenschaften von Seltenerdionen wurden mittels Absorptions- und Emissionsspektroskopie untersucht. Eu^{3+} und Tb^{3+} erwiesen sich als geeignete Indikatorionen zur Charakterisierung der lokalen Umgebung der Seltenerdionen. Er^{3+} und Nd^{3+} finden breite Anwendung in Lasern und Verstärkern. Die Kenntnis des Einflusses der Wirtsglasmatrix auf die spektroskopischen Eigenschaften von Seltenerdionen ermöglichte die Modellierung der Emissionseigenschaften bedeutender Übergänge von Er^{3+} und Nd^{3+}, um optimale Wirtsgläser herauszufinden. Fluorid-Phosphat- und Phosphatgläser sind attraktive Wirtsmaterialien für Laser und Verstärker. Der Kovalenzgrad zwischen Seltenerdionen und Liganden in diesen Gläsern hat einen dominierenden Einfluß auf die spektroskopischen Parameter von Seltenerdionen wie Judd-Ofelt-Parameter und Elektronen-Phononen-Kopplungskonstante. Der Anstieg der Elektronen-Phononen-Kopplungskonstante mit dem Phosphatgehalt ist für die Abnahme der Er^{3+} Emissionsintensität bei 540 nm verantwortlich. Andererseits führt es zu einer Zunahme der Er^{3+} Emissionsintensität bei 1,5 µm. Die geringeren Mikroparameter der Nd^{3+} Kreuzrelaxation in Phosphatgläsern verglichen mit Fluorid-Phosphat-Gläsern bewirken eine Erhöhung der Lebensdauer des $^4F_{3/2}$ Laserniveaus von Nd^{3+} bei höheren Nd^{3+} Konzentrationen. Der Energietransfer zu OH-Gruppen in Phosphatgläsern vermindert die Lebensdauer und Emissionsintensität des Laserniveaus sowohl von Er^{3+} als auch Nd^{3+}.

1. Introduction

The optical properties of rare earth ions are widely used in lasers, amplifiers, upconversion devices, scintillators and Faraday rotators [1 to 5]. Fluoride phosphate and phosphate glasses are attractive host materials for the active ions [1 and 6]. The varied, radiative and non-radiative transitions of the rare earth ions between the 4f levels extend from the ultraviolet to the infrared spectral region [1, 7 and 8]. Therefore, absorption and emission spectroscopy is an useful tool for characterization of the rare earth ions in glasses. The knowledge of the relationships between host glasses and rare earth ions is essential to design glasses for definite applications.

The spectroscopic properties of the rare earth ions are affected by the host glass composition. Local structure and bonding features are covalency, asymmetry, coordination number and distance to the ligands of the rare earth sites [1 and 8 to 11]. Further, long range effects such as rigidity and ionic packing ratio have an influence on the spectroscopic properties [12 to 14]. The incorporation of the rare earth ions in the glasses can vary from random distribution up to formation of rare earth pairs or clusters. On the other side, spectroscopic properties of rare earth ions can used to investigate the local structure and bonding around them.

Important parameters of radiative transitions are the Judd-Ofelt parameters. They are phenomenological characteristics for the influence of the host matrix on the absorption and emission properties of the rare earth ions [8 and 15]. Non-radiative transitions are multiphonon and energy transfer processes. Multiphonon relaxation is affected by the electron-phonon coupling strength and phonon energy of the host matrix [16 and 17]. Cross relaxation is an energy transfer process between one type of rare earth ions. It plays an important role at higher rare earth concentrations [18 to 21]. Its probability

Received 2 April, 1998.

[1)] Presented in German at: 71st Annual Meeting of the German Society of Glass Technology (DGG) on May 27, 1997 in Bayreuth (Germany).

Table 1. Batch compositions of the investigated glasses (Ln = Eu, Tb, Nd, Er).

glass	batch composition in mol%
FP x	$x\ Sr(PO_3)_2 \cdot (100-x)\ [MgF_2, CaF_2, SrF_2, AlF_3, LnF_3]$
SrP	$(100-x)\ Sr(PO_3)_2 \cdot x\ Ln(PO_3)_3$
KLaP	$40\ KPO_3 \cdot (60-x)\ La(PO_3)_3 \cdot x\ Ln(PO_3)_3$
KBaP	$35\ KPO_3 \cdot 45\ Ba(PO_3)_2 \cdot (20-x)\ Al(PO_3)_3 \cdot x\ Ln(PO_3)_3$

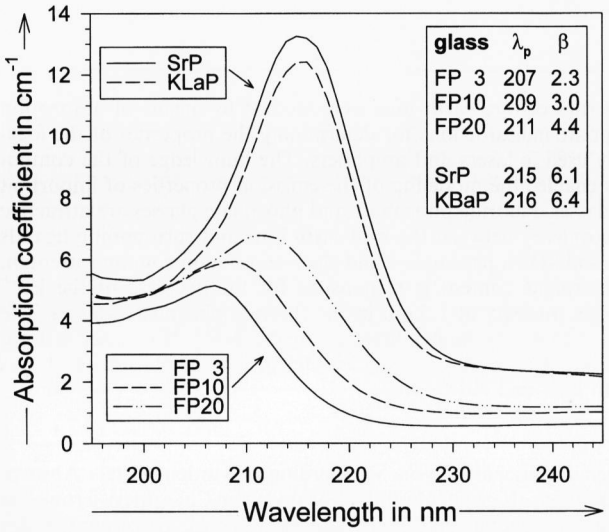

Figure 1. Absorption spectra, peak wavelength λ_p in nm and nephelauxetic ratio β in 10^{-2} of Tb^{3+} $4f^8 \rightarrow 4f^75d^1$ transition.

depends on the distance and multipolar interaction between the rare earth ions. The distance is given by the distribution of the rare earth ions in the matrix. The interaction is characterized by the so-called microparameter of energy transfer processes [22]. In phosphate glasses, energy transfer to OH groups occurs due to comparatively high OH contents [19, 21, 23 and 24].

In this paper, both relationships between host glass composition and spectroscopic properties of rare earth ions are studied for fluoride phosphate and phosphate glasses. Tb^{3+} and Eu^{3+} are used as indicator ions for local structure investigations. The nephelauxetic shift of the Tb^{3+} f→d absorption band serves as a measure of covalency between the rare earth ions and ligands. From Eu^{3+} absorption spectra, structure-sensitive Judd-Ofelt parameters were determined. Electron-phonon coupling strength and phonon energy of the host glass are obtained from phonon sidebands of Eu^{3+} $^7F_0 \rightarrow {}^5D_2$ transition. The emission decay of the Tb^{3+} $^5G_6 \cdot {}^5D_3 \rightarrow {}^7F_6$ transitions is used for examination of the cross relaxation between the Tb^{3+} ions theirselves and of energy transfer to OH groups. The influence of host glass composition on the spectroscopic parameters and the relationships between the different parameters is studied. On the basis of these results, the influence of host glass composition on the emission properties of important Er^{3+} and Nd^{3+} transitions could be revealed. The Er^{3+} emission at 540 nm is attractive for upconversion laser devices pumped with infrared laser diodes [25 and 26]. The Er^{3+} emission at 1.5 µm is used in fibre optics and optical amplifiers for the telecommunication [2 and 27]. From the metastable $^4F_{3/2}$ state of Nd^{3+}, two attractive emissions occur. The one at 1.06 µm is used for solid state lasers [1, 18 and 28]. The other at 1.3 µm is recently of interest for fibre optics and optical amplifiers in the telecommunication [29].

2. Experimentals

The compositions of the fluoride phosphate (FP) and phosphate (P) glasses investigated in this study are given in table 1. The preparation of the samples is reported in references [19, 23 and 30]. The measurements for determining the spectroscopic properties of Tb^{3+} and Eu^{3+} ions are described in references [21 and 30]. The experimental arrangements of the Er^{3+} and Nd^{3+} emission measurements are given in references [19 and 23].

3. Properties of the local environment and relationships between the spectroscopic parameters of rare earth ions

3.1 Nephelauxetic ratio of Tb^{3+} f→d absorption

The nephelauxetic shift of the Tb^{3+} $4f^8 \rightarrow 4f^75d^1$ absorption band at 210 nm serves as a measure of the covalency between rare earth ions and surrounding ligands. The nephelauxetic ratio, β, is defined as [7]

$$\beta = (\tilde{\nu}_f - \tilde{\nu})/\tilde{\nu}_f \quad (1)$$

where $\tilde{\nu}_f$ is the peak wave number of the absorption band of the free ion, and $\tilde{\nu}$ is the one of the ion in the solid. For Tb^{3+} the value of the free ion is unknown. Thus, the value of Tb^{3+} in LaF_3 [31] is used as $\tilde{\nu}_f$. For the investigated glasses, both the peak wavelength and nephelauxetic ratio of Tb^{3+} f→d absorption band increase with increasing phosphate content. The peak wavelength and nephelauxetic ratio of the KLaP glass tend to higher values compared with the SrP glass (figure 1). These results are ascribed to increasing covalency between rare earth ions and ligands due to increasing polarizability of the ligands. As the phosphate content increases, fluorine ions having lower polarizability are substituted by oxygen ions having higher polarizability.

In the KLaP glass, the presence of K^+ ions having low field strength is responsible for the higher polarizability of the oxygens around the rare earth ions.

3.2 Judd-Ofelt Ω_t parameters

The structure-sensitive Judd-Ofelt Ω_t parameters of Eu^{3+} were determined from absorption spectra as described in [30]. The Ω_2 parameter increases with increasing covalency and asymmetry at the rare earth sites [8]. The influence of covalency on Ω_2 results from the decreasing effect of covalency on the energy difference between the 4f and 5d states of the rare earth ions [32]. The degree of covalency is determined from the nephelauxetic ratio of the Tb^{3+} f→d absorption band. The linear increase of Ω_2 with increasing nephelauxetic ratio (figure 2) indicates the predominant influence of covalency on the Ω_2 parameter in the glasses investigated.

Ω_6 depends on the covalency in another way than Ω_2. It is more affected by the radial integral between the 4f and 5d states of the rare earth ions. Increasing σ-electron donation from the ligands to the rare earth ions within the σ-bonds decreases the radial integral and thus Ω_6 [10, 11]. Accordingly, higher polarizability of the ligands should result in lower Ω_6. In fact, the lower Ω_6 parameters of the P glasses with respect to the FP glasses, as well as the lower Ω_6 parameter of the KLaP glass compared with the SrP glass (figure 3) correlate with the increase of the ligand polarizability in the same order, detected by Tb^{3+} f→d nephelauxetic ratio. By contrast, the π-electron donation from the resonating double bonds within the PO_4-tetrahedra to the 5d orbitals of the rare earth ions increases the 5d electron density and, consequently, the Ω_6 parameter [10, 11]. In the FP glasses, Ω_6 tends to larger values with increasing phosphate content (figure 3) despite increasing amount of oxygens as σ-electron donors. This indicates slightly greater influence of the π-electron donation on Ω_6 compared with the σ-electron donation.

The Ω_4 parameter is affected by the factors causing changes in both Ω_2 and Ω_6.

3.3 Electron-phonon coupling strength and phonon energy

The electron-phonon coupling strength and phonon energy of the glasses were determined from phonon sideband spectra as described in [30]. In the FP glasses, one phonon sideband is observed. It has a phonon energy of about 1090 cm^{-1} and is attributed to diphosphate groups. In the P glasses, two phonon sidebands are found. They are ascribed to the symmetric and asymmetric stretching vibration of PO_2 groups within the polyphosphate chains. The corresponding phonon energies are about 1150 and 1300 cm^{-1}, respectively. The electron-phonon coupling strength, determined from these phonon sidebands, increases with increasing Tb^{3+} f→d nephelauxetic ratio (figure 4). This indicates that the increase of covalency between rare earth ions and oxygen ions of the phosphate groups leads to stronger interaction between the 4f electrons of the rare earth ions and the phonons of the neighboring phosphate groups.

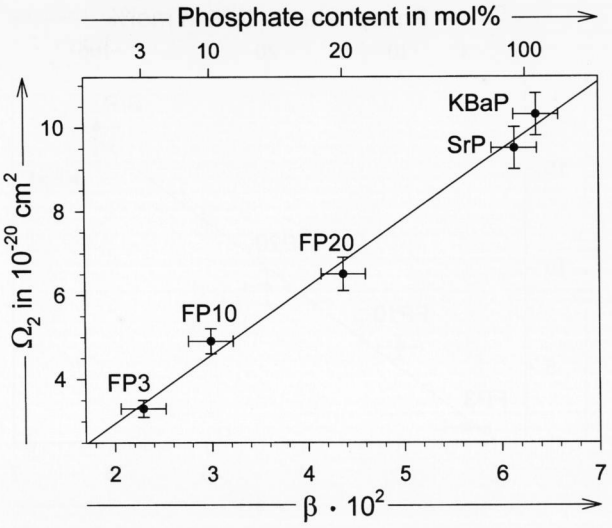

Figure 2. Judd-Ofelt Ω_2 parameter of Eu^{3+} as a function of Tb^{3+} f→d nephelauxetic ratio β. The line is obtained by linear regression.

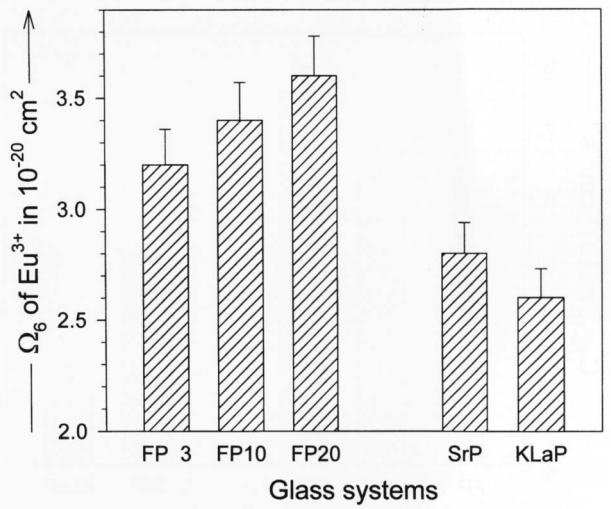

Figure 3. Judd-Ofelt Ω_6 parameter of Eu^{3+} in various glasses.

3.4 Microparameter of Tb^{3+} cross relaxation

In the case of Tb^{3+}, resonant cross relaxation between excited and non-excited Tb^{3+} ions occurs [20 and 33]. The microparameter of this energy transfer process was determined from Tb^{3+} emission decay measurements. The emission at 380 nm reflects the transitions from the $^5D_3$ and thermally populated $^5G_6$ levels to the $^7F_6$ ground state [33]. The two excited states are depopulated by Tb^{3+} cross relaxation. This is indicated by non-exponential decay of these states for the samples doped with (1 to 50) · 10^{19} Tb^{3+} cm^{-3}. All decay curves could

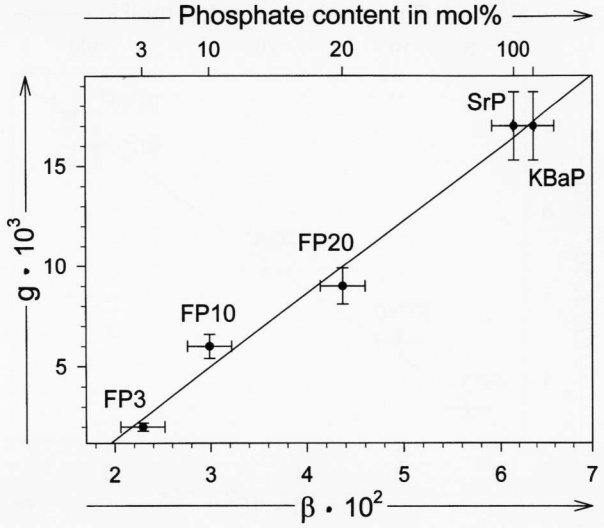

Figure 4. Electron-phonon coupling strength g as a function of Tb^{3+} f→d nephelauxetic ratio β. The line is obtained by linear regression.

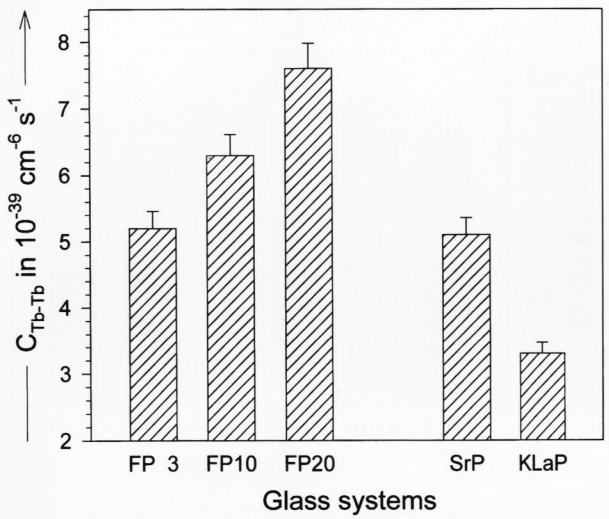

Figure 5. Microparameter of Tb^{3+} cross relaxation C_{Tb-Tb} in various glasses.

be well fitted by the Inokuti-Hirayama model assuming dipole-dipole interaction between donor and acceptor [34 and 35],

$$I(t) = I(0)\exp(-t/\tau_D - B\sqrt{t}) \tag{2}$$

$$B = 4/3\,\pi^{3/2} N_A \sqrt{C_{DA}} \tag{3}$$

where $1/\tau_D$ is the decay rate of the donor in the absence of acceptor ions, N_A is the concentration of the acceptor ions, and C_{DA} is the microparameter of the energy transfer process as described in detail in chapter 4. The validity of this model for the investigated glasses suggests random spatial distribution of Tb^{3+} ions in the host glass matrices. The two adjustable parameters, $1/\tau_D$ and B, were determined by least-squares fitting procedure. From the linear dependence of the B parameter on the Tb^{3+} concentration, N_{Tb}, the microparameter of the Tb^{3+} cross relaxation, C_{Tb-Tb}, was determined according to equation (3) by

$$B_{Tb} = 4/3\,\pi^{3/2} N_{Tb} \sqrt{C_{Tb-Tb}}. \tag{4}$$

In the case of the P glasses, energy transfer from the two excited states to OH groups additionally occurs. Therefore, the B parameter depends on the concentration of both acceptors, Tb^{3+} ions and OH groups. The microparameters of Tb^{3+} cross relaxation and of energy transfer to OH groups were determined from the linear dependence of B on the Tb^{3+} concentration and the OH content by

$$B = 4/3\,\pi^{3/2}(N_{Tb}\sqrt{C_{Tb-Tb}} + N_{OH}\sqrt{C_{Tb-OH}}). \tag{5}$$

The microparameters of the Tb^{3+} cross relaxation are shown in figure 5 for the investigated glass systems. In general, the microparameter of a dipole-dipole energy transfer process depends on the oscillator strengths of the donor and acceptor transitions which increases with increasing Judd-Ofelt Ω_t parameters. Furthermore, the spectral overlap between the donor emission and acceptor absorption bands has an influence on the microparameter [22] (chapter 4). Increasing linewidth of the transition bands is assumed to increase the spectral overlap. For both Tb^{3+} cross relaxation and energy transfer to OH groups, the $^5G_6 \cdot {}^5D_3 \rightarrow {}^5D_4$ transitions represent the donor transitions. They are dependent on all Ω_t parameters [36]. In the case of cross relaxation, the $^7F_6 \rightarrow {}^7F_0$ transition of Tb^{3+} serves as acceptor transition. It solely depends on Ω_6 since the matrix elements corresponding to Ω_2 and Ω_4 are zero [37]. In the case of Tb−OH transfer, the first overtone of the OH stretching vibration interacts with the Tb^{3+} donor transition. The compositional dependence of Ω_t is described above. In the FP glasses, the increase of the microparameter with the phosphate content (figure 5) is due to the increase of all Ω_t parameters. This effect gives rise to both acceptor and donor oscillator strengths. The lower microparameters in the P glasses compared with the FP glasses result from the lower Ω_6 parameters (figure 3) and linewidths of the acceptor transition (figure 6). The former influence leads to a lower oscillator strength of the acceptor transition. The latter one decreases the overlap between donor and acceptor transition bands. The decrease of the microparameter in the KLaP glass compared with the SrP glass is caused by the decrease of the Ω_6 parameter and of the linewidth of the acceptor transition, too.

4. Influence of the compositional dependence of spectroscopic parameters on Er^{3+} and Nd^{3+} emission properties

4.1 Er^{3+} emission at 540 nm

The emission spectra of the Er^{3+} $^4S_{3/2} \rightarrow {}^4I_{15/2}$ emission at 540 nm were recorded by direct pumping into the $^2H_{11/2}$ level at 520 nm. The intensity normalized to the total Er^{3+} concentration decreases to a large extent with increasing phosphate content and to a lower extent with increasing Er^{3+} concentration of the investigated glasses (figure 7). In order to figure out the different influences on the 540 nm emission, the measured values of the steady state intensity were fitted with different models involving radiative decay, multiphonon relaxation and cross relaxation.

The intensity, F_{ij}, of an emission transition $i \rightarrow j$ is proportional to the spontaneous emission probability, A_{ij}, of the transition and the population density of the excited state, N_i, [38].

$$F_{ij} \sim A_{ij} N_i \tag{6}$$

The normalization to the total Er^{3+} concentration, N_{Er}, gives

$$F_{ij}/N_{Er} \sim A_{ij} n_{ij} \tag{7}$$

$$n_i = N_i/N_{Er} \,. \tag{8}$$

The relative populations, n_i, can be determined from rate equations. This requires the consideration of the processes involved in the population and relaxation of the Er^{3+} levels.

The decrease of the normalized emission intensity with increasing Er^{3+} concentration suggests the occurence of non-radiative cross relaxation between the Er^{3+} ions. The probability of resonant energy transfer process in the case of dipole-dipole interaction depends on the microparameter, C_{DA}, of the donor-acceptor interaction and on the distance, R_{DA}, between donor and acceptor ions [22]

$$W_{DA} = C_{DA}/R_{DA}^6 \,. \tag{9}$$

Since homogeneous distribution of rare earth ions was found from the study of Tb^{3+} cross relaxation, the distance is approximated from the Er^{3+} concentration by

$$1/R_{DA}^3 = N_{Er} \,. \tag{10}$$

The microparameter is proportional to the oscillator strengths, P_D and P_A, of the donor and acceptor transitions, $J_D \rightarrow J'_D$ and $J_A \rightarrow J'_A$, [22].

$$C_{DA} = \frac{3e^4}{8\pi^2 m^2} \frac{1}{\tilde{\nu}_{DA}^2} \frac{1}{n^2} P_D P_A \int f_D(\tilde{\nu}) f_A(\tilde{\nu}) \, d\tilde{\nu} \tag{11}$$

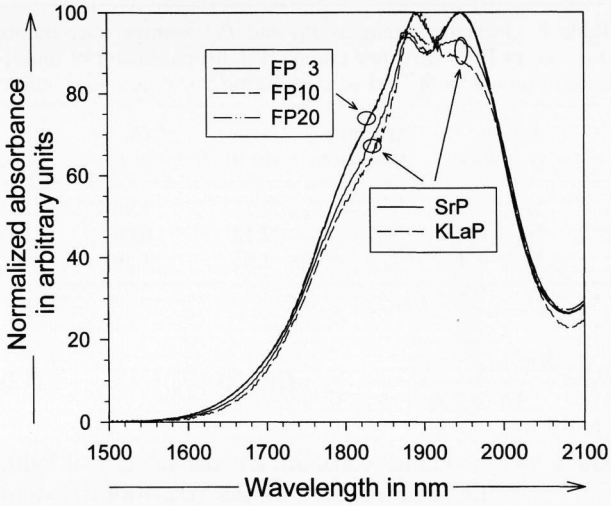

Figure 6. Normalized absorption spectra of Tb^{3+} $^7F_6 \rightarrow {}^7F_{0,1,2}$ transitions in various glasses.

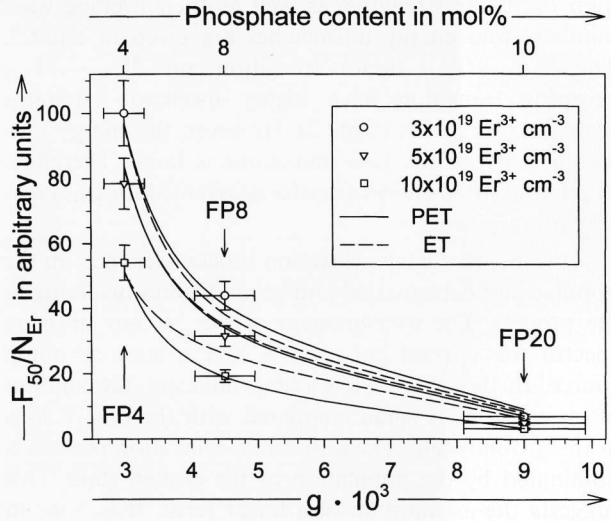

Figure 7. Er^{3+} emission intensity at 540 nm normalized to the total Er^{3+} concentration F_{50}/N_{Er} as a function of electron-phonon coupling strength g in fluoride phosphate glasses with different Er^{3+} concentrations. The solid lines are obtained by least-squares fitting procedure of the model assuming phonon-assisted energy transfer (PET). The dashed lines are obtained from the model assuming resonant energy transfer (ET).

where D denotes the donor, and A denotes the acceptor; e is the electron charge given in electrostatic units, m is the electron mass, and n is the refractive index. $\tilde{\nu}_{DA}$ is taken as the average wave number of the transitions involved in the transfer process. $\int f_D(\tilde{\nu}) f_A(\tilde{\nu}) \, d\tilde{\nu}$ is the overlap of the normalized lineshape functions for the emission of the donor ions and the absorption of the acceptor ions. The oscillator strengths, $P_k (k = D, A)$, are given by the Judd-Ofelt theory as [39 and 40]

Table 2. Oscillator strengths P_D and P_A, average wave number $\tilde{\nu}_{DA}$ and energy mismatch $\Delta\tilde{\nu}$ of donor and acceptor transitions involved in Er^{3+} cross relaxation. $W_{MP}^{fit}(0)$ parameter of multiphonon relaxation and C_{DA}^{fit} microparameter of Er^{3+} cross relaxation, both obtained from least-squares fitting procedure. C_{DA}^{calc} microparameter calculated according to equation (11).

	donor transition	acceptor transition	P_D in 10^{-6}	P_A in 10^{-6}	$\tilde{\nu}_{DA}$ in cm^{-1}	$\Delta\tilde{\nu}$ in cm^{-1}	$W_{MP}^{fit}(0)$ in $10^{11}\ s^{-1}$	C_{DA}^{fit} in $10^{-39}\ cm^6\ s^{-1}$	C_{DA}^{calc} in $10^{-39}\ cm^6\ s^{-1}$
a	$^4S_{3/2}\rightarrow{}^4I_{13/2}$	$^4I_{15/2}\rightarrow{}^4F_{9/2}$	2.13	1.90	13600	3500	1	0.1	1.0
b	$^4S_{3/2}\rightarrow{}^4I_{13/2}$	$^4I_{15/2}\rightarrow{}^4I_{11/2}$	2.13	0.60	11020	1570	5	2000	0.6
c	$^4S_{3/2}\rightarrow{}^4I_{9/2}$	$^4I_{15/2}\rightarrow{}^4I_{13/2}$	1.03	1.36	6270	650	5	2000	2.0

$$P_k = \frac{8\pi^2 m c}{3h}\,\frac{\tilde{\nu}_k}{2J_k+1}\sum_{t=2,4,6}\Omega_t^{(k)}\,\langle\|U_t^{(k)}\|\rangle^2 \qquad (12)$$

where h is the Planck constant, c is the velocity of light, and $\tilde{\nu}_k$ is the wave number of the transition. Ω_t and $\langle\|U_t\|\rangle^2$ are the parameters and matrix elements of the Judd-Ofelt treatment. The oscillator strengths were calculated from the Ω_t parameters of the glasses reported in reference [32] and from the matrix elements reported in references [41 and 42] for different donor and acceptor transitions. Er^{3+} cross relaxation transitions of high oscillator strengths, as well as their average wave numbers and energy mismatches are given in table 2. The $^4S_{3/2}\rightarrow{}^4I_{13/2}$ donor transition and $^4I_{15/2}\rightarrow{}^4F_{9/2}$ acceptor transition have higher oscillator strengths than the other ones (table 2). However, the energy mismatch between the two transitions is large. Therefore, phonon-assisted energy transfer is assumed for this cross relaxation process.

In general, a cross relaxation process depends on the population of the excited and ground states involving in the process. The measurement of the 540 nm emission spectra was carried out using a Xenon lamp as pump source. In this case of low pump intensity, the amount of excited ions is small compared with the one of ions in the ground state. Then, the cross relaxation process is dominated by the population of the excited state. This suggests the assumption of a linear term, $W_{DA}\cdot n_5$, in the rate equations.

In the present case of 540 nm emission, the $^4S_{3/2}$ excited state is immediately populated by fast non-radiative phonon decay from the $^2H_{11/2}$ pump level. Considering the cross relaxation process, $^4S_{3/2}\rightarrow{}^4I_{13/2}/{}^4I_{15/2}\rightarrow{}^4F_{9/2}$, with the highest oscillator strengths and taking into account the low pump intensity, the rate equations are expressed as

$$dn_5/dt = Gn_0 - (A_5 + W_5 + W_C)n_5 \qquad (13)$$

$$dn_4/dt = (A_{54} + W_5 + W_C)n_5 - (A_4 + W_4)n_4 \qquad (14)$$

$$dn_3/dt = A_{53}n_5 + (A_{43} + W_4)n_4 - (A_3 + W_3)n_3 \qquad (15)$$

$$dn_2/dt = A_{52}n_5 + A_{42}n_4 + (A_{32} + W_3)n_3 - (A_2 + W_2)n_2 \qquad (16)$$

$$dn_1/dt = (A_{51} + W_C)n_5 + A_{41}n_4 + A_{31}n_3 + (A_{21} + W_2)n_2 - (A_1 + W_1)n_1 \qquad (17)$$

where: the subscripts 0 to 5 denote the energy states from $^4I_{15/2}$ to $^4S_{3/2}$, A_i are the total radiative decay rates of the states i, A_{ij} are the spontaneous emission probabilities of the transitions $i\rightarrow j$, W_i are the multiphonon relaxation rates of the states i, G is the pump rate, and W_C is the cross relaxation rate.

The radiative decay rates, A_i and A_{ij}, were calculated from the Ω_t parameters of the investigated glasses as reported in reference [32].

The multiphonon relaxation rates were estimated from [17 and 43]

$$W_{MP}(\Delta E) = W_{MP}(0)\exp(-\alpha\Delta E) \qquad (18)$$

$$\alpha = \frac{1}{\hbar\omega}\left(\ln\frac{\Delta E}{\hbar\omega\, g} - 1\right) \qquad (19)$$

where ΔE is the energy gap between the neighboring states of multiphonon decay, $\hbar\omega$ is the maximum phonon energy of the host glass, and g is the electron-phonon coupling strength. For calculation of the term $\exp(-\alpha\Delta E)$, the parameters, $\hbar\omega$ and g, were estimated from phonon sidebands measurements as portrayed in chapter 3. ΔE was obtained from the barycenters of the absorption bands of the excited states. $W_{MP}(0)$ remains as adjustable parameter which is assumed to be equal for the host glasses investigated. From the known values of $W_{MP}(0)$ for phosphate glasses [16 and 44], the value in the present case is estimated to ranges from $5\cdot10^{10}$ to $5\cdot10^{11}\ s^{-1}$.

According to the equations (9) and (10), W_C in the case of resonant energy transfer is given by

$$W_{C,ET} = C_{DA}\,N_{Er}^2 . \qquad (20)$$

Phonon-assisted energy transfer is expressed as [43 and 45]

$$W_{C,PET}(\Delta E) = W(0)\exp(-\alpha\Delta E)\exp(\gamma\Delta E) \qquad (21)$$

$$\gamma = (1/\hbar\omega)\ln 2 . \qquad (22)$$

Since energy transfer and multiphonon process are involved in the phonon-assisted energy transfer, $W(0)$ is assumed to include the probabilities extrapolated to zero energy gap for both processes. These are the resonant transfer rate and the $W_{MP}(0)$ parameter of multiphonon relaxation as given in equation (18).

$$W(0) = W_{C,ET}\, W_{MP}(0) \tag{23}$$

In summary, $W_{C,PET}$ is expressed as

$$W_{C,PET}(\Delta E) = C_{DA}\, N_{Er}^2\, W_{MP}(0) \exp(-\alpha \Delta E) \exp(\gamma \Delta E)\,. \tag{24}$$

The influence of the host glass composition on the cross relaxation microparameter, C_{DA}, is estimated from the compositional dependence of the oscillator strengths according to equation (11). The spectral overlap is approximated to be constant. The normalization of the values for the three FP host glasses to the one of the FP4 glass gives a parameter, k_C, which portrays the increase of C_{DA} with increasing phosphate content,

$$C_{DA} = C \cdot k_C \tag{25}$$

where C is an adjustable parameter in the fit procedure. The pump rate, W_{Pump}, is defined as [46]

$$W_{Pump} = 2.303\, \frac{(E/t)\, \sigma_P}{h\nu_P\, a} \tag{26}$$

where E/t is the power of the pump source, σ_P is the absorption cross section at the pump wavelength, $h\nu_P$ is the energy of one pump photon, and a is the area of the pump beam. From the specification of the experimental equipment, W_{Pump} is calculated to be about 10 s^{-1}. The increase of the absorption cross section with the phosphate content of the glasses and the decrease of the pump light absorption in the sample with increasing penetration of the pump light is taken into account by a factor k_A. Then the overall pump rate, G, is given by

$$G = k_A\, W_{Pump}\,. \tag{27}$$

With regard to the reabsorption of the emission light by a correction factor k_F depending on the absorption cross section of the glasses at the emission wavelength, the measured emission intensity at 540 nm, F_{50}, is modeled by

$$F_{50}/N_{Er} = z_5\, k_F\, A_{50}\, n_5 \tag{28}$$

where z_5 is an adjustable constant of the experimental equipment. The excited state population, n_5, is determined from steady state rate equations $dn_i/dt = 0$. In the expressions for the transition probabilities, involved in the rate equations, and in the expression (28) for the emission intensity, the A_i, A_{ij}, $\exp(-\alpha_i \Delta E_i)$, $\exp(\gamma \Delta E)$, k_C, k_A, k_F, W_{Pump} parameters were calculated, while the z_5, $W_{MP}(0)$ and C parameters were adjustable ones.

The observed values for the emission could be well fitted with the rate equations (13) to (17) assuming phonon-assisted energy transfer. It could not be well fitted assuming resonant energy transfer $^4S_{3/2} \rightarrow {}^4I_{13/2}/{}^4I_{15/2} \rightarrow {}^4I_{11/2}$ and $^4S_{3/2} \rightarrow {}^4I_{9/2}/{}^4I_{15/2} \rightarrow {}^4I_{13/2}$, respectively. The observed values and fitted curves according to phonon-assisted energy transfer are shown in figure 7 as a function of electron-phonon coupling strength and Er^{3+} concentration. Those of resonant energy transfer are also reported in figure 7. In the case of phonon-assisted energy transfer, $W_{MP}(0) = 1 \cdot 10^{11}$ s^{-1} and $C = 1 \cdot 10^{-40}$ $cm^6\, s^{-1}$ were obtained by the fitting procedure. The calculated value of C_{DA} for the FP4 glass assuming full overlap between donor and acceptor band of 200 cm^{-1} linewidth is about $1 \cdot 10^{-39}$ $cm^6\, s^{-1}$. In the case of resonant energy transfer, the fitted values for $W_{MP}(0)$ and C are $5 \cdot 10^{11}$ s^{-1} and $2 \cdot 10^{-36}$ $cm^6\, s^{-1}$, respectively. The latter one does not agree with the calculated values of $6 \cdot 10^{-40}$ $cm^6\, s^{-1}$ and $2 \cdot 10^{-39}$ $cm^6\, s^{-1}$ for the energy transfer processes (b) and (c) in table 2, respectively.

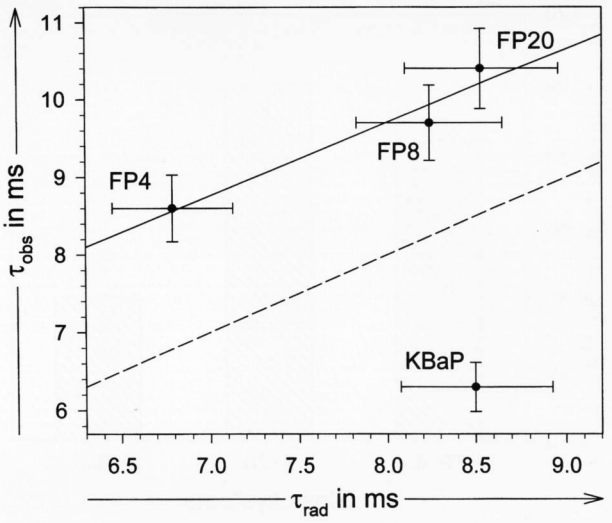

Figure 8. Observed lifetime of the Er^{3+} $^4I_{13/2}$ state τ_{obs} as a function of the radiative one τ_{rad} determined by Judd-Ofelt analysis. The solid line is obtained by linear regression. On the dashed line, the observed lifetime is equal to the radiative one.

The modeling of the emission intensity indicates the large influence of the electron-phonon coupling strength on the 540 nm emission. The increase of the coupling strength with the phosphate content mainly causes the decrease of the 540 nm emission intensity with the phosphate content. Further, it leads to an increase of the cross relaxation probability. In comparison, the compositional changes of the radiative decay rates and of the cross relaxation microparameter have only a small influence on the emission intensity.

4.2 Er^{3+} emission at 1.5 μm

In the FP glasses, the observed lifetime of the $^4I_{13/2}$ excited state of the 1.5 μm emission slightly increases with the phosphate content of the glasses (figure 8). Because of the large energy gap to the neighboring $^4I_{15/2}$ ground state, multiphonon relaxation from $^4I_{13/2}$ calculated according to equations (18) and (19) is negligible in the investigated glasses. Thus, the decay of the $^4I_{13/2}$ state should be solely radiative. In fact, the increase of the observed lifetime from FP4 to FP20 glass agrees with

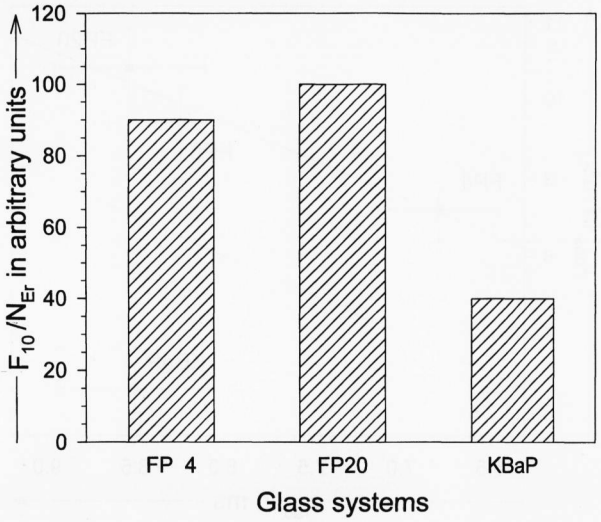

Figure 9. Er^{3+} emission intensity at 1.5 µm normalized to the total Er^{3+} concentration F_{10}/N_{Er} in various glasses.

the increase of the radiative lifetime calculated from the Judd-Ofelt parameters [32]. The higher values of the observed lifetime, τ_{obs}, for all FP glasses are due to radiation trapping whose probability, W_{Trap}, is given by [47]

$$1/\tau_{obs} = A_{10} - W_{Trap} \,. \tag{29}$$

The mean value found for W_{Trap} is $(23 \pm 7)\ s^{-1}$. The observed lifetime of the P glasses is clearly lower than that of the FP glasses (figure 8). However, the radiative lifetime is in the same magnitude. The decrease of the lifetime is attributed to the comparatively high OH content of the P glass. The absorption coefficient of the OH stretching vibration at about 3000 cm^{-1} which serves as a measure of the OH content [48] ranges from 3 to 6 cm^{-1} in these glasses. By contrast, the absorption coefficient of the FP glasses at 3000 cm^{-1} is lower than 0.1 cm^{-1}. The high OH content enables energy transfer from the Er^{3+} $^4I_{13/2}$ state to the first overtone of the OH stretching vibration. This additional decay process causes the lower lifetime observed in the P glasses. Using W_{Trap} obtained from the FP glasses, the probability of the energy transfer to OH groups, W_{OH}, was calculated from

$$1/\tau_{obs} = A_{10} - W_{Trap} + W_{OH} \tag{30}$$

to be $(64 \pm 7)\ s^{-1}$.

Neglecting radiation trapping due to the experimental equipment, the observed lifetime of $^4I_{13/2}$ in the FP glasses is governed by radiative decay. The radiative lifetime of the glasses is comparatively high, ranging from 6 to 9 ms. Therefore, fluoride phosphate glasses are attractive candidates for lasers and amplifiers. By contrast, the decay in the phosphate glasses occurs additionally via energy transfer to OH groups. The resulting decrease of the observed lifetime diminishes the potential of these glasses.

The emission spectra of the Er^{3+} $^4I_{13/2} \rightarrow {}^4I_{15/2}$ transition at 1.5 µm were recorded by pumping into the $^4F_{9/2}$ level at 650 nm. The intensity normalized to the total Er^{3+} concentration slightly increases from the FP4 glass to the FP20 glass having higher phosphate content. The intensity of the KBaP glass is considerably lower than those of the FP glasses (figure 9).

Similar to the emission at 540 nm, the intensity, F_{10}, at 1.5 µm was modeled on the basis of the expression (7) using rate equations for determination of the excited state population, n_1.

$$F_{10}/N_{Er} = z_1 A_{10} n_1 \tag{31}$$

Because the normalized intensity is found to be nearly independent of the Er^{3+} concentration in the range of $(3 \text{ to } 10) \cdot 10^{19}\ Er^{3+}\ cm^{-3}$, cross relaxation and other concentration quenching processes are negligible. Thus, the rate equations can be expressed as follows.

$$dn_4/dt = Gn_0 - (A_4 + W_4)n_4 \tag{32}$$

$$dn_3/dt = (A_{43} + W_4)n_4 - (A_3 + W_3)n_3 \tag{33}$$

$$dn_2/dt = A_{42}n_4 + (A_{32} + W_3)n_3 - (A_2 + W_2)n_2 \tag{34}$$

$$dn_1/dt = A_{41}n_4 + A_{31}n_3 + (A_{21} + W_2)n_2 - (A_1 + W_1)n_1 \tag{35}$$

As reported for the 540 nm emission, the radiative decay rates and the $\exp(-\alpha_i \Delta E_i)$ terms of the multiphonon relaxation rates are known parameters. The unknown $W_{MP}(0)$ parameter of the multiphonon relaxation rates was calculated from the observed emission intensities at 1.5 µm. The value is about $5 \cdot 10^{11}\ s^{-1}$. In comparison, the $W_{MP}(0)$ parameter obtained from the modeling of the 540 nm emission amounts $1 \cdot 10^{11}\ s^{-1}$. However, the experimental values of the 540 nm emission intensity could also be well fitted by $W_{MP}(0) = 5 \cdot 10^{11}\ s^{-1}$. The relative differences between the modeled values of these two fitting procedures are lower than 15%.

The modeling of the 1.5 µm emission indicates that the intensities are governed by the population rate of the $^4I_{13/2}$ state via multiphonon relaxation. The increase of the electron-phonon coupling strength with increasing phosphate content results in a faster population of the $^4I_{13/2}$ state from the $^4I_{11/2}$ level. The $^4I_{11/2} \rightarrow {}^4I_{15/2}$ emission which does not lead to a population of the $^4I_{13/2}$ state decreases. Consequently, the emission intensity at 1.5 µm increases with increasing phosphate content of the FP glasses. Therefore, the FP20 glass is the most attractive host for Er^{3+} lasers and amplifiers at 1.5 µm.

In the P glasses, energy transfer from $^4I_{13/2}$ to OH groups occurs additionally in the decay of $^4I_{13/2}$

$$dn_1/dt = A_{41}n_4 + A_{31}n_3 + (A_{21} + W_2)n_2 - (A_1 + W_1 + W_{OH})n_1 \,. \tag{36}$$

Using $W_{MP}(0)$ determined from the FP glasses and W_{OH} obtained from the lifetime measurements, the calculated emission intensity of the KBaP glass with respect to the FP20 glass is about 60%. The observed intensity amounts 40%. The modeling indicates that the $^4F_{9/2}$, $^4I_{9/2}$ and $^4I_{11/2}$ states in the FP20 and KBaP glasses predominantly decay non-radiatively to the $^4I_{13/2}$ state because of their high multiphonon relaxation rates. The additional depopulation of $^4I_{13/2}$ via energy transfer to OH groups in the KBaP glass with respect to the FP20 glass causes the lower emission intensity which is observed in the former one.

4.3 Lifetime of the Nd^{3+} $^4F_{3/2}$ laser state

The lifetime of the metastable $^4F_{3/2}$ laser state of Nd^{3+} decreases with increasing Nd^{3+} concentration due to the presence of cross relaxation between the Nd^{3+} ions. From the dependence of the observed lifetime on the Nd^{3+} concentration, a parameter, k_{cross}, was determined which serves as a measure of the microparameter of Nd^{3+} cross relaxation [19]. This parameter exhibits the same tendencies by variation of the host glass like the microparameter of Tb^{3+} cross relaxation (figure 10). In the case of the Nd^{3+} cross relaxation, $^4F_{3/2} \rightarrow {}^4I_{15/2}/{}^4I_{9/2} \rightarrow {}^4I_{15/2}$, both donor and acceptor transitions depend solely on Ω_6. The other two Ω_t parameters do not have any influence on the transitions because the corresponding matrix elements are zero [41 and 49]. The decrease of Ω_6 in the order FP20 > SrP > KLaP governs the decrease of k_{cross} in the same order. Furthermore, a decrease of the linewidths as observed for Tb^{3+} is assumed to be responsible for the decrease of k_{cross}. In phosphate glasses, energy transfer from $^4F_{3/2}$ to OH groups occurs, which decreases the lifetime of the laser state [19]. Nevertheless, phosphate glasses are attractive hosts at higher Nd^{3+} concentrations due to their lower microparameters of cross relaxation. Provided the OH content is decreased to an absorption coefficient of at least 3 cm^{-1} by the melting procedure, they possess higher lifetimes at $>4 \cdot 10^{20}$ Nd^{3+} cm^{-3} than the FP20 fluoride phosphate glass (figure 11).

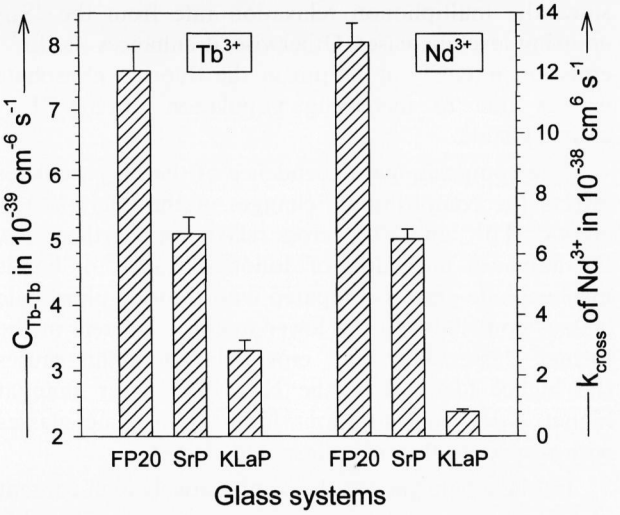

Figure 10. Microparameter of Tb^{3+} cross relaxation C_{Tb-Tb} and k_{cross} parameter of Nd^{3+} cross relaxation in various glasses.

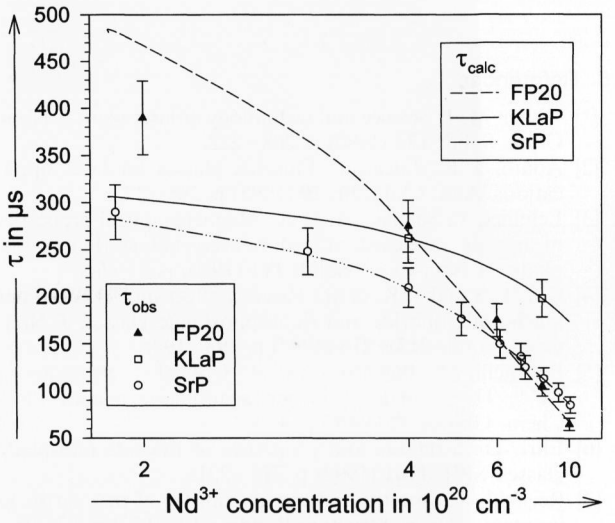

Figure 11. Lifetime of the Nd^{3+} $^4F_{3/2}$ state τ as a function of Nd^{3+} concentration. The dots are observed values. The ones in phosphate glasses are corrected to an OH content corresponding to an absorption coefficient of 3 cm^{-1} at 3000 cm^{-1}. The lines are modeled curves according to [19].

5. Summary and Conclusions

The relationships between host glass composition and optical properties of rare earth ions were studied by means of absorption and emission spectroscopy. Several spectroscopic properties of the indicator ions, Eu^{3+} and Tb^{3+}, were found to be an useful tool for determining the properties of the local environment around rare earth ions. Knowing the compositional dependence of the spectroscopic parameters, the emission properties of important Er^{3+} and Nd^{3+} transitions could be modeled in order to figure out the influence of host glass matrices.

Fluoride phosphate and phosphate glasses are attractive candidates for lasers and amplifiers. In these glasses, the degree of covalency between the rare earth ions and surrounding ligands is important. It increases with increasing phosphate content and at presence of modifier ions having low field strength due to the increase of the ligand polarizability. As a result, the Tb^{3+} f→d nephelauxetic ratio, Eu^{3+} Ω_2 parameter and electron-phonon coupling strength are enhanced, whereas Ω_6 of phosphate glasses is lower than that of fluoride phosphate glasses. The slight increase of Ω_6 in fluoride phosphate glasses with the phosphate content is attributed to an increase of the π-electron donation from PO_4 units.

The increase of the electron-phonon coupling strength with the phosphate content is responsible for the decrease of the Er^{3+} emission intensity at 540 nm,

since the multiphonon relaxation rate from the $^4S_{3/2}$ emitting level increases. Otherwise, it enhances the Er^{3+} emission intensity at 1.5 µm in the fluoride phosphate glasses due to increasing population of the $^4I_{13/2}$ emitting state.

The compositional dependence of the Ω_6 parameter affects the compositional changes of the microparameters of Tb^{3+} and Nb^{3+} cross relaxation. Furthermore, the narrower linewidths of donor and acceptor bands in phosphate glasses compared with fluoride phosphate glasses contribute to the lower microparameters in the former glasses. For Nd^{3+} cross relaxation, this causes the higher lifetimes of the Nd^{3+} $^4F_{3/2}$ laser state at higher Nd^{3+} concentrations in the phosphate glasses with respect to fluoride phosphate glasses.

In phosphate glasses, the comparatively high content of OH groups results in energy transfer from suitable excited states of rare earth ions to OH groups. This decreases the lifetime and emission intensity of the $^4I_{13/2}$ laser state of Er^{3+}, as well as the lifetime of the $^4F_{3/2}$ laser state of Nd^{3+}.

6. References

[1] Weber, M. J.: Science and technology of laser glass. J. Non-Cryst. Solids **123** (1990) p. 208–222,

[2] Adam, J. L.; Lucas. J.: Fluoride glasses for laser applications. Ann. Chim. Fr. **20** (1995) p. 261–272.

[3] Letellier, V.; Seignac, A. et al.: Magneto-optical properties of heavily rare-earth doped non-crystalline fluorophosphates. J. Non-Cryst. Solids **111** (1990) p. 55–62.

[4] Qiu, J.; Tanaka, K. et al.: Faraday effect in Tb^{3+}-containing borate, fluoride and fluorophosphate glasses. J. Non-Cryst. Solids **213&214** (1997) p. 193–198.

[5] Bettinelli, M.; Ingletto, G. et al.: Optical spectroscopy of Ce^{3+}, Tb^{3+} and Eu^{3+} in new scintillating glasses. Phys. Chem. Glasses **37** (1996) p. 4–8.

[6] Ehrt, D.: Structure and properties of fluoride phosphate glasses. SPIE **1761** (1992) p. 213–221.

[7] Reisfeld, R.: Spectra and energy transfer of rare earths in inorganic glasses. Structure Bonding **13** (1973) p. 53–98.

[8] Reisfeld, R.: Radiative and non-radiative transitions of rare earth ions in glasses. Structure Bonding **22** (1975) p. 123–175.

[9] Wang, J.; Brocklesby, W. S. et al.: Local structures of rare earth ions in glasses: the 'crystal-chemistry' approach. J. Non-Cryst. Solids **163** (1993) p. 261–267.

[10] Tanabe, S.; Hanada, T. et al.: Correlation between ^{151}Eu Mössbauer isomer shift and Judd-Ofelt Ω_6 parameters of Nd^{3+} ions in phosphate and silicate laser glasses. Phys. Rev. B **48** (1993) p. 10591–10594.

[11] Tanabe, S.; Ohyagi, T. et al.: Relation between the Ω_6 intensity parameter of Er^{3+} ions and the ^{151}Eu isomer shift in oxide glasses. J. Appl. Phys. **73** (1993) p. 8451–8454.

[12] Jørgensen, C. K.; Reisfeld, R.: Judd-Ofelt parameters and chemical bonding. J. Less-Common Metals **96** (1983) p. 107–112.

[13] Takebe, H.; Morinaga, K. et al.: Correlation between radiative transition probabilities of rare-earth ions and composition in oxide glasses. J. Non-Cryst. Solids **178** (1994) p. 58–63.

[14] Takebe, H.; Nageno, Y. et al.: Compositional dependence of Judd-Ofelt parameters in silicate, borate, and phosphate glasses. J. Am. Ceram. Soc. **78** (1995) p. 1161–1168.

[15] Peacock, R. D.: The intensities of lanthanide f-f transitions. Structure Bonding **22** (1975) p. 83–122.

[16] Layne C. B.; Lowdermilk, W. H.; Weber, M. J.: Multiphonon relaxation of rare-earth ions in oxide glasses. Phys. Rev. B **16** (1977) p. 10–20.

[17] Toratani, H.; Izumitani, T.; Kuroda, H.: Compositional dependence of nonradiative decay rate in Nd laser glasses. J. Non-Cryst. Solids **52** (1982) p. 303–313.

[18] Caird, J. A.; Pamponi, A. J.; Staver, P. R.: Quantum efficiency and excited-state relaxation dynamics in neodymium-doped phosphate laser glasses. J. Opt. Soc. Am. B **8** (1991) p. 1391–1403.

[19] Ebendorff-Heidepriem, H.; Seeber, W.; Ehrt, D.: Spectroscopic properties of Nd^{3+} ions in phosphate glasses. J. Non-Cryst. Solids **183** (1995) p. 191–200.

[20] Hayakawa, T.; Kamata, N.; Yamada, K.: Visible emission characteristics in Tb^{3+}-doped fluorescent glasses under selective excitation. J. Lumin. **68** (1996) p. 176–186.

[21] Ebendorff-Heidepriem, H.; Ehrt, D.: Structure investigations of glasses by examination of spectroscopic properties of Eu^{3+} and Tb^{3+} ions. Proc. Fundamentals of Glass Science and Technology 1997, Växjö, Sweden, p. 500–505.

[22] Henderson, B.; Imbusch, G. F.: Optical spectroscopy of inorganic solids. Monographs on the physics and chemistry of materials, Clarendon Press, Oxford, 1989.

[23] Ebendorff-Heidepriem, H.; Seeber, W.; Ehrt, D.: Spectroscopic investigations of the Er^{3+} fluorescence transitions at 540 nm and 1.5 µm in fluoride phosphate and phosphate glasses. Glastech. Ber. Glass Sci. Technol. **66** (1993) no. 9, p. 235–244.

[24] Yan, Y.; Faber A. J.; de Waal H.: Luminescence quenching by OH groups in highly Er-doped phosphate glasses. J. Non-Cryst. Solids **181** (1995) p. 283–290.

[25] Takahashi, M.; Shojiva, R. et al.: Nonradiative decay processes and mechanisms of frequency upconversion of Er^{3+} in ZrF_4–BaF_2–LaF_3 glass. J. Appl. Phys. **81** (1997) p. 2940–2945.

[26] Lu, Y.-L.; Lu, Y.-Q.; Ming, N.-B.: Fluorescence and attenuation properties of Er^{3+}-doped phosphate-glass fibers and efficient infrared-to-visible up-conversion. Appl. Phys. B **81** (1996) p. 287–291.

[27] Taccheo, S.; Laporta, P. et al.: Diode-pumped bulk erbium-ytterbium lasers. Appl. Phys. B **63** (1996) p. 425–436.

[28] Marion, J. E.; Weber, M. J.: Phosphate laser glasses. Eur. J. Solid State Inorg. Chem. **28** (1991) p. 271–287.

[29] Ishikawa, E.; Aoki, H. et al.: Laser emission and amplification of 1.3 µm in Neodymium-doped fluorophosphate fibres. Electronics Letters **28** (1992) p. 1497–1499.

[30] Ebendorff-Heidepriem, H.; Ehrt, D.: Spectroscopic properties of Eu^{3+} and Tb^{3+} ions for local structure investigations of fluoride phosphate and phosphate glasses. J. Non-Cryst. Solids **208** (1996) p. 205–216.

[31] Krupa, J. C.; Queffelec, M.: UV and VUV optical excitations in wide band gap materials doped with rare earth ions. J. Alloys Comps. **250** (1997) p. 287–292.

[32] Ebendorff-Heidepriem, H.; Ehrt, D.: Affect of glass composition on Judd-Ofelt parameters and radiative decay rates of Er^{3+} in fluoride phosphate and phosphate glasses. J. Non-Cryst. Solids **240** (1998) p. 66–78.

[33] Duhamel-Henry, N.; Adam, J. L. et al.: Photoluminescence of new fluorophosphate glasses containing a high concentration of terbium(III) ions. Opt. Mat. **5** (1996) p. 197–207.

[34] Inokuti, M.; Hirayama, F.: Influence of energy transfer by the exchange mechanism on donor luminescence. J. Chem. Phys. **43** (1963) p. 1978–1989.

[35] Stokowski, S. E.; Krashkevich, D.: Transition-metal ions in Nd-doped glasses. Spectra and effects on Nd fluorescence. Materials Research Society Symposium Proceedings **61** (1986) p. 273–282.

[36] Caird, J. A.; Carnall, W. T.; Hessler, J. P.: The terbium chloride – aluminium chloride vapor system. III. Spectral intensity analysis. J. Chem. Phys. **74** (1981) p. 3225–3233.

[37] Carnall, W. T.; Fields, P. R.; Rajnak, K.: Electronic energy levels of the trivalent lanthanide aquo ions. III. Tb^{3+}. J. Chem. Phys. **49** (1969) p. 4447–4449.
[38] Pollnau, M.; Heumann, E. et al.: Experimental determination of radiative-transition rates and quantum efficiencies in Er^{3+}; $YAlO_3$. Opt. Commun. **118** (1995) p. 250–254.
[39] Judd, B. R.: Optical Absorption intensities of rare-earth ions. Phys. Rev. **127** (1962) p. 750–761.
[40] Ofelt, G. S.: Intensities of crystal spectra of rare-earth ions. J. Chem. Phys. **37** (1962) p. 511–520.
[41] Carnall, W. T.; Fields, P. R.; Rajnak, K.: Electronic energy levels in the trivalent lanthanide aquo ions. I. Pr^{3+}, Nd^{3+}, Pm^{3+}, Sm^{3+}, Dy^{3+}, Ho^{3+}, Er^{3+}, and Tm^{3+}. J. Chem. Phys. **49** (1968) p. 4424–4442.
[42] Carnall, W. T.: Crosswhite, H.; Crosswhite, H. M.: Energy level structure and transition probabilities of the trivalent lanthanides in LaF_3. Argonne Natl. Lab. Rept., 1977.
[43] Miyakawa, T.; Dexter, D. L.: Phonon sidebands, multiphonon relaxation of excited states, and phonon-assisted energy transfer between ions in solids. Phys. Rev. B **1** (1970) p. 2961–2969.
[44] Reisfeld, R.: Excited state phenomena in vitreous materials. Handbook on the Physics and Chemistry of Rare earths, edited by K. A. Gschneidner, Jr. and L. Eyring, Elsevier Science Publisher B.V., 1987.
[45] Soga, K.; Tsuda, M. et al.: Effects of chloride introduction on the optical properties and the upconversion emission at 980-nm excitation of Er^{3+} in ZBLAN fluoride glasses. J. Non-Cryst. Solids **222** (1995) p. 272–281.
[46] Shi, W. Q.; Bass, M.; Birnbaum, M.: Effects of energy transfer among Er^{3+} ions on the fluorescence decay and lasing properties of heavily doped $Er:Y_3Al_5O_{12}$. J. Opt. Soc. Am. B **7** (1990) p. 1456–1462.
[47] Li, C.; Wyon, C.; Moncorgé, R.: Spectroscopic properties and fluorescence dynamics of Er^{3+} and Yb^{3+} in Y_2SiO_5. IEEE J. Quant. Electron. *28* (1992) P. 1209–1221.
[48] Ebendorff-Heidepriem, H.; Ehrt, D.: Determination of the OH content of glasses. Glastech. Ber. Glass Sci. Technol. **68** no. 5, p. 139–146.
[49] Krupke, W. F.: Induced-emission cross sections in neodymium laser glasses. IEEE J. Quant. Electron. **4** (1974) p. 450–457.

1098P001

Address of the authors:

H. Ebendorff-Heidepriem, D. Ehrt
Friedrich-Schiller-Universität
Otto-Schott-Institut für Glaschemie
Fraunhoferstraße 6
D-07743 Jena